International Journal of
Plasma Environmental Science and Technology

Regular Paper

DOI: 10.34343/ijpest.2022.16.e03003

Characteristics of high-speed mist generated by condensation of water vapor in pressurized air

Yunchen Xiao[1,2], Siwei Liu[1], Tomoki Nakajima[1], Takehiko Sato[1]

[1] Institute of Fluid Science, Tohoku University, Japan
[2] Graduate School of Engineering, Tohoku University, Japan

* Corresponding author: takehiko.sato.d7@tohoku.ac.jp (Takehiko Sato)

Received: 28 July 2022
Revised: 27 October 2022
Accepted: 31 October 2022
Published online: 4 November 2022

Abstract

The application of droplets has been extensively discussed and explored for decades. The cleaning effect, which is based on the typical application of droplets, requires small droplets and high droplet velocities to improve cleaning efficiency. In this study, a high-speed mist-generating device was developed based on the condensation of water vapor in pressurized air. It can stably produce high-speed mist with nanoscale droplets. Several experiments were conducted to determine mist characteristics. The cleaning effect was validated by cleaning process indicators, which proved that the mist can clean the surface within 10 s. The temperature and pressure distributions were measured. Then, the mist velocity in the range of 35–49 mm along the *x*-direction was estimated to be 52–65 m s^{-1} at 35 mm and 40–51 m s^{-1} at 49 mm. The mist at the nozzle exit was determined to be a supersonic flow based on the Schlieren visualization. Moreover, electric current was detected on the aluminum plate, which was set downstream. The current decreases with an increase in the distance from the nozzle exit and increases with an increase in the inlet gas pressure.

Keywords: Supersonic flow, pressure, temperature, cleaning, charge generation.

1. Introduction

Oral health is increasingly being focused owing to the increase in the public awareness of personal oral hygiene [1, 2]. Plaque is the primary cause of dental diseases (e.g., gingivitis and periodontal diseases); therefore, plaque removal is of great importance and has been widely studied [3]. As per reports, tooth brushing, which has been commonly applied to remove plaque for decades [4–6], cannot reach the interdental areas between adjacent teeth, and the teeth can be damaged owing to overbrushing [3,7]. Several novel cleaning methods have been developed and evaluated in recent years [8, 9]. Among these cleaning methods, the use of high-speed microdroplets, a micro-size droplet with high velocity, is assumed to be a potential, effective way of removing dental plaque [10, 11]. In our previous study, the removal mechanism of microdroplets from artificial dental plaque was experimentally evaluated [12]. Plaque was removed by applying normal stress instead of shear stress. However, as the size of the droplets is relatively large in the test, it may cause collateral damage to the surface, in addition to removing the dental plaque. Previous results proved that the cleaning efficiency with regard to the application of droplets is more related to velocity than the diameter, and the efficiency is high for small droplets with respect to their volume [13]. In addition, charges were detected in the mist flow, which was expected to change the characteristics of the target object (e.g., electric potentials, surface conditions, dielectric properties, and others). Therefore, it is reasonable to predict a significant cleaning effect of the high-speed mist and expect to improve cleaning efficiency using small droplets.

In this study, a high-speed mist generation device was developed based on the condensation of water vapor in pressurized air. In contrast to our previous study, the condensation of water vapor in pressurized air generates high-speed mist of smaller size and higher velocity, which is assumed to improve the cleaning effect. The characteristics of high-speed mist were investigated based on the following aspects: (1) cleaning efficiency, (2) temperature distribution, (3) pressure and velocity distribution, (4) the visualization of the dynamics of the flow near the nozzle, and (5) the electrical property of the mist droplet. The results validated the cleaning effect of the high-speed mist.

2. Experimental setup

The mist-generating device is shown in Fig.1 (a). It comprised a heater (AS ONE Corporation, EHP-170N) and stainless steel water vessel with an inlet for pressurized gas and an outlet for mist. A thermocouple (represented as T in Fig. 1), heater, and relay (not shown here) were used to construct the PID feedback control system. This system helps stabilize the temperature of the water vessel, so that sufficient energy for evaporation, but not excess energy for explosive boiling, can be applied to the vessel. The total amount of water was 200 mL in one test, and it was heated to continuously evaporate; the temperature was fixed to the boiling point temperature at a specific saturated vapor pressure. As a reference, in this study, an inlet pressure of 5 atm and water temperature of 152.3 °C were considered as the standard conditions, and it can stably generate high-speed mist for ~35 min.

The mixture of water vapor and pressurized gas flowed through a nozzle (Spraying Systems Co., HB-1/8-VV-SS-15-01) (Fig. 1 (d)). During this process, the water vapor condenses owing to the rapid decrease in temperature and finally forms a large number of small droplets. This type of mixture is defined as high-speed mist in this study. To stabilize the nozzle temperature, the outlet pipe and nozzle were continuously heated with a wire heater at 30 W (Tokyo Technological Labo, CRX-1).

The Schlieren visualization system was constructed downstream of the mist (Fig. 1 (b)). It comprised a xenon lamp (KATOKOKEN CO, LTD, LS-300), two convex lenses, a knife, and a camera (Nikon, D4). The visualization was carefully implemented. The xenon lamp was at the focus of the first convex lens (f = 300 mm), which transferred the point light into parallel light. The nozzle was placed in this parallel light region, and the mist flowed perpendicular to the light. The parallel light was focused on one knife by the second convex lens (f = 200 mm), and a part of the light was separated by the knife to generate Schlieren images.

The electrical current detection system is shown in Fig. 1 (c). An aluminum plate (50×45×2 mm) was placed in front of the nozzle at distance *d*. An electrometer (KEITHLEY 6517A) was used to measure the electric current from the plate to the ground. The current was measured and recorded at different distances, *d*, and inlet gas pressures, *p*.

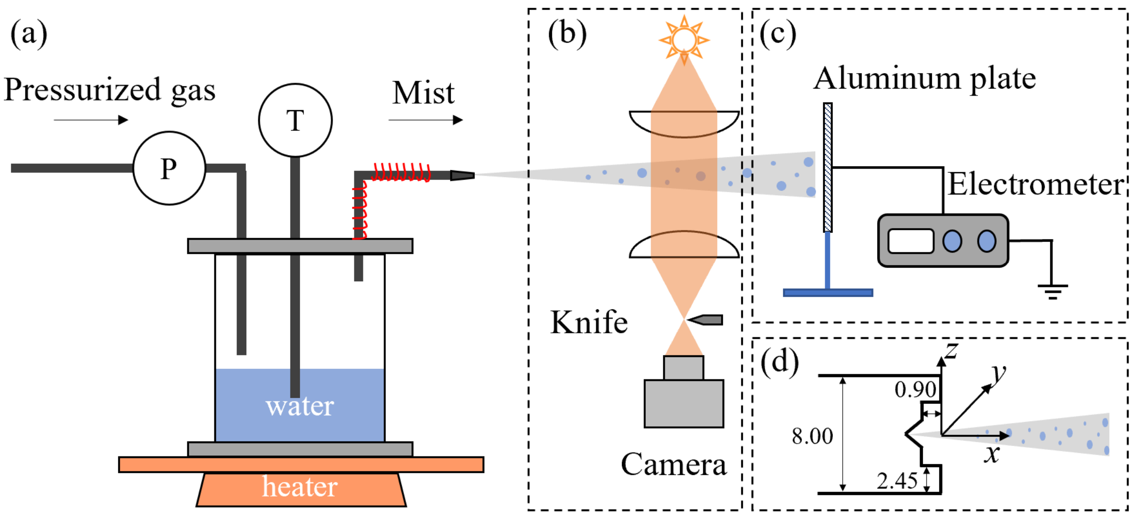

Fig. 1. Schematic of the mist-generating device and test platform. (a) High-speed mist-generating device. P denotes the pressure gauge, T denotes the temperature meter. (b) Schlieren visualization system. (c) Electric current detection system. (d) Primary size of the nozzle and the definitions of three axes in this study. Note: the Schlieren visualization system (b) and the Electric current detection system (c) are not applied at the same time, and all results in the following sections were acquired by using the two systems individually.

3. Results and discussion

3.1 Cleaning efficiency of high-speed mist

The cleaning process indicator (gke-GmbH, gke Clean-Record® cleaning process indicator W-CPI-Y) was used to verify the cleaning effect of the high-speed mist. The index to be evaluated is whether the organic material coated on the indicator (yellow parts in Fig. 2) can be removed by the impact of the mist. The indicator was fixed at a specified position, and a stepping motor stage (SIGMAKOKI CO., LTD, SGSP26-100) with a single-axis stage controller (SIGMAKOKI CO., LTD, GSC-01) was used to control the exposure time of the indicator toward the mist. For each condition, the indicator was exposed to mist three times. The images of the indicators with different statuses after exposure to the mist are shown in Fig. 2. If the impact region of the indicator turned from yellow to white, it indicated a strong cleaning effect. Therefore, it was denoted as the "effectively cleaned" status and marked as "+" in the results. Otherwise, if the region is "not effectively cleaned, it was marked as "–" and regarded as the "no cleaning effect" status.

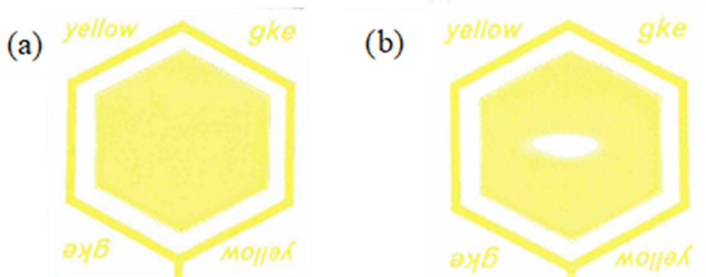

Fig. 2. Pictures of the indicators with different statuses. (a) No cleaning effect status. In this case, there is no region of effectively cleaned. This status will be marked as – in Table 1 and Table 2. (b) Effectively cleaned status. In this case, the impact region of the indicator turned to be white from yellow, indicating a strong cleaning effect. This status will be marked as + in Table 1 and Table 2.

The cleaning effects of the mist at different inlet gas pressures and distances are summarized in Tables 1 and 2. The material on the indicator was completely removed in less than 10 s at a distance of 1 cm from the nozzle when the gas pressure was greater than 4 atm. However, the mist flow did not exhibit any cleaning effect at 2 and 3 atm for an exposure time of 10 s. Even for an exposure time of 60 s, the mist did not exhibit a strong cleaning effect at $p = 2$ or 3 atm. It is assumed that the cleaning mechanism is related to the collision process, which requires a detailed microscopic observation. Further studies are required to address this issue.

Table 1. Indicator status at different pressure and different position with an exposure time of 10 s.

Pressure \ Position	10 mm	20 mm	30 mm
2 atm	– – –	– – –	– – –
3 atm	– – –	– – –	– – –
4 atm	+ + +	– – –	– – –
5 atm	+ + +	+ + +	– – –

Table 2. Indicator status at different pressure and different position with an exposure time of 60 s.

Pressure \ Position	10 mm	20 mm	30 mm
2 atm	– – –	– – –	– – –
3 atm	– – –	– – –	– – –
4 atm	+ + +	– + –	– – –
5 atm	+ + +	– + +	– – –

3.2 Distributions of total temperature and pressure

The total temperature and pressure distributions of the mist are considered to be important parameters if the developed device can be used for practical applications (e.g., dental cleaning requires a moderate temperature for the patient). A dramatic decrease in temperature and pressure is expected after the mist leaves the nozzle, particularly for safety reasons. The spatial distributions of the total temperature and pressure of the high-speed mist were measured and are discussed in this section. A thermocouple was fixed at the 3-axis moveable stage, and the total temperatures at different positions were measured. As shown in Fig. 1 (d), the *x*, *y*, and *z* directions denote the downstream, horizontal, and vertical directions. The total temperature distribution is shown in Fig. 3. The mist near the nozzle remained at a high temperature, and its temperature rapidly decreased with an increase in the distance along the *x* direction owing to the strong heat transfer. The temperature stabilized in the range of 35–49 mm along the *x* direction. The temperature distributions along the *y* and *z* directions were relatively symmetric. However, the thermocouple setup inevitably affects the flow characteristics, thus affecting the temperature measurement. In future studies, we will consider this case and improve our results using non-invasive methods.

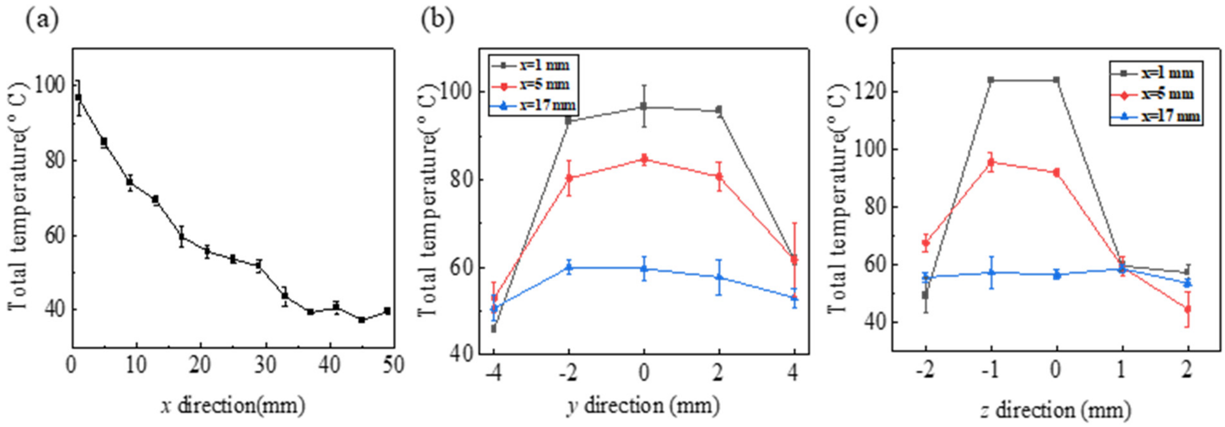

Fig. 3. The total temperature distribution along three directions with an inlet gas pressure of 5 atm. (a) The distribution along the *x*-direction; (b) The distribution along the y-direction; (c) The distribution along the *z*-direction.

The pressure distribution of the mist flow with an inlet gas pressure of 5 atm was measured using a pitot tube (LK-00, OKANO WORKS, Ltd.) and flow meter (FV-21, OKANO WORKS, Ltd.). Owing to the performance limitation of the flow meter, pressures in the range of 0–2 kPa can be detected. Therefore, the pressure at each downstream position (3.5, 3.7, 3.9, 4.1, 4.3, 4.5, 4.7, and 4.9 cm) was measured repetitively. The pressure value at each point was measured three times and averaged to determine the pressure variation with respect to the position. The distributions of dynamic pressure, static pressure, and total pressure are shown in Fig. 4. The dynamic pressure (Fig. 4 (a)) and total pressure (Fig. 4 (b)) were directly measured using the pitot tube, and the static pressure (Fig. 4 (c)) was acquired by subtracting the former results.

The droplets in the experiment of this study could not be observed using the high-speed camera, as evident in our previous study [12], indicating much smaller droplet sizes. It was difficult to directly estimate the droplet velocity using optical images. However, the droplets in the mist can be accelerated or decelerated by the surrounding gas and can eventually reach a stable velocity. The droplet velocity mainly depended on the mist velocity. Therefore, the gas flow velocity, which is regarded as an index of droplet velocity in this study, can be calculated based on the pressure distribution of the mist [14, 15].

The mist density should not be regarded as constant owing to its compressibility upon pressure or expandability based on heat. Therefore, the mist density affected by temperature and pressure is defined by equation (1).

$$\rho = \rho_0 \left(\frac{273}{273+\theta}\right) \times \frac{101.3+P_S}{101.3} \quad (1)$$

where ρ_0 denotes the density of the fluid at 20 °C, θ denotes the gas temperature, and p_s denotes the static pressure, which is expressed in kPa. Based on the static pressure distribution shown in Fig. 4 (c), we can consider that compressibility is negligible. Thus, density is the function of the temperature distribution.

Then, the mist velocity can be roughly estimated using the dynamic pressure value and Equation (2).

$$v = \sqrt{2 \times p_\mathrm{d}/\rho} \tag{2}$$

where p_d denotes the dynamic pressure.

Based on the temperature distribution shown in Fig. 3, the temperature reaches a relatively stable value in the range of 35–49 mm along the x direction, maintained at ~40 °C. The density of water vapor is 0.7122 kg m^{-3} at 40 °C, and the density of dry air is 1.128 kg m^{-3} at 40 °C. The velocities of vapor and air can be estimated using the dynamic pressure distribution illustrated in Fig. 4 (a) and its density at 40 °C, and the calculated results are illustrated in Fig. 4 (d). It is assumed that the high-speed mist is a mixture of dry air and water vapor, and the mist density should be interposed between the two values. Therefore, it is reasonable to assume that the mist velocity in the range of 35–49 mm along the x direction can be predicted to be between the velocity lines of the vapor and air, as shown in Fig. 4 (d).

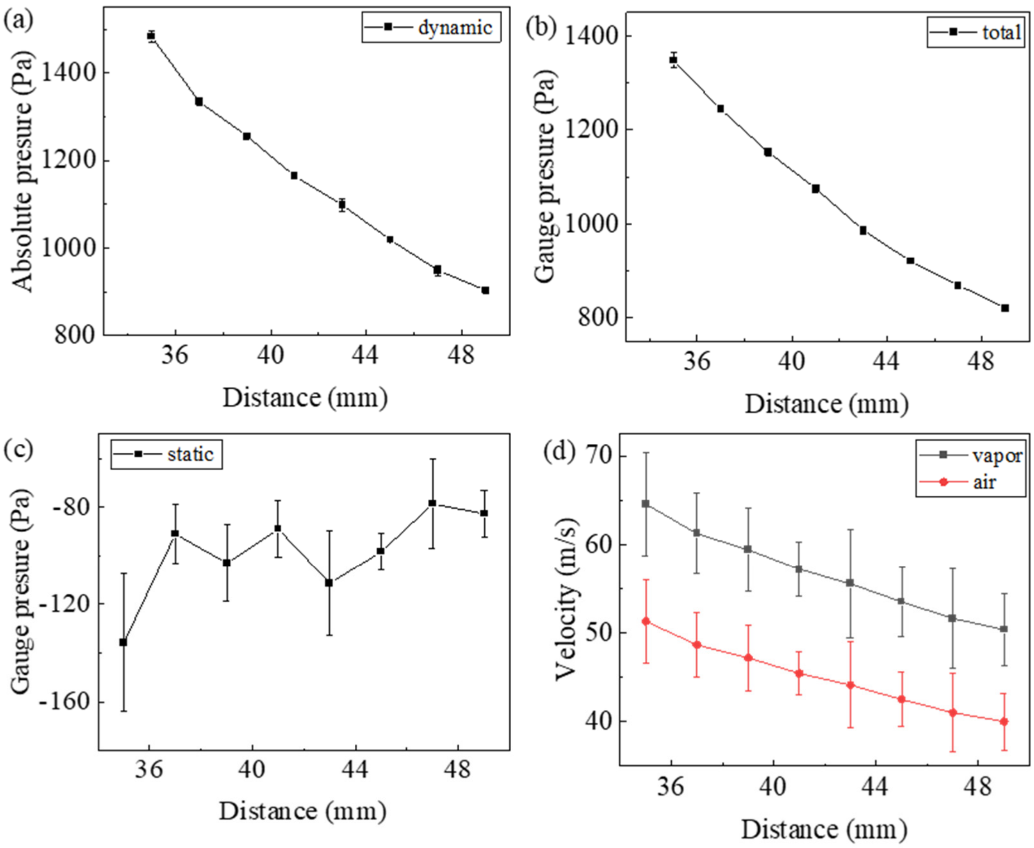

Fig. 4. The pressure distribution and velocity distribution of the mist from 35 to 49 mm at p = 5 atm. (a) Dynamic pressure of the flow as a function of distance; (b) Total pressure of the flow as a function of distance; (c) Static pressure calculated as a function of distance; (d) Velocity of the flow estimated from dynamic pressure.

3.3 Visualization of the mist flow

The supersonic flow of the high-speed mist at the nozzle exit was observed using the Schlieren method (Fig. 5). The characteristics and patterns of the flow are influenced by the experimental layout (e.g., nozzle design and pressure). In our case, the pressure at the nozzle exit (5 atm, as illustrated in Fig. 5) was much larger than the ambient pressure; thus, an underexpanded supersonic flow was formed upon leaving the nozzle exit (Fig. 5 (a)). The Schlieren images of the high-speed mist at the nozzle exit are shown in Figs. 5 (b) and (c). Fig. 5 (b) shows the gas flow before heating, and Fig. 5 (c) shows the mist flow after heating. Although the Schlieren images are not clear, it is still possible to recognize the Mach dish in the flow, as shown in Figs. 5 (b) and (c).

It is reasonable to conclude that the gas and mist leaving the nozzle exit are supersonic. However, the patterns of the gas and mist flows are slightly different in terms of horizontal length and vertical expansion. The mist flow is shorter in the supersonic region, indicating a faster decrease in velocity compared to the gas flow. The velocity decrease may have been caused by the condensation and cooling of the mist flow. As the supersonic flow expands, the temperature of the supersonic flow decreases; thus, water vapor condenses into water droplets. The water vapor space was filled with the surrounding air. The introduction of the surrounding air caused a decrease in the average velocity of the mist flow. Consequently, the length of the supersonic region decreased for the mist flow.

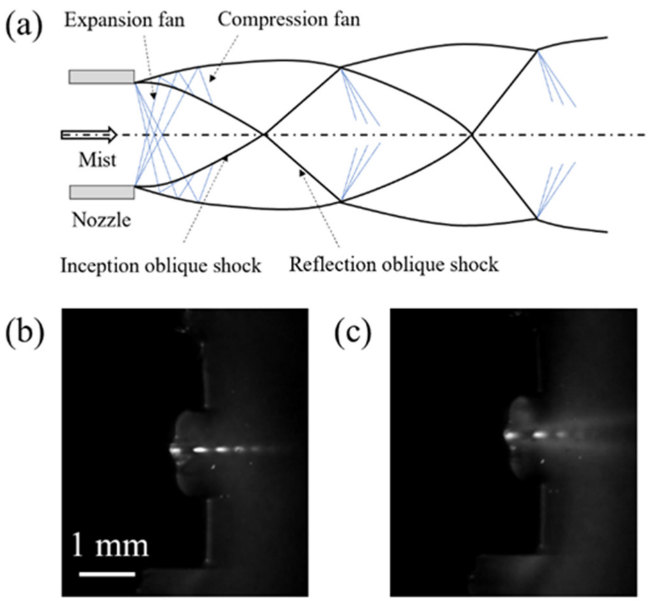

Fig. 5. Supersonic flow of the high-speed mist at the nozzle exit. (a) Schematic pattern of the underexpanded supersonic flow. (b) Schlieren image of the gas flow with p = 5 atm at the nozzle exit. (c) Schlieren image of the mist flow with p = 5 atm at the nozzle exit.

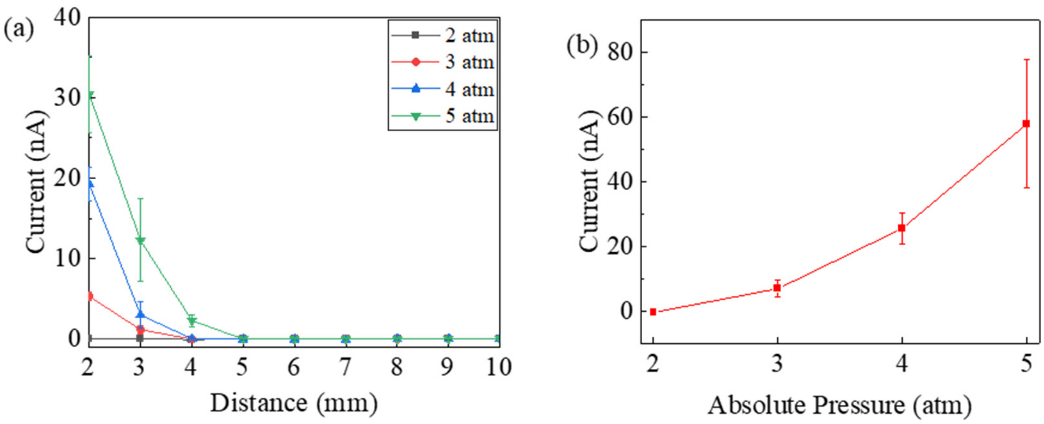

Fig. 6. (a) Mist current as a function of distance at p = 2, 3, 4 and 5 atm; (b) Mist current as a function of pressure at x = 2 mm.

3.4 Mist current

Charges were detected in the high-speed mist during the experiment. Charged droplets are expected to significantly affect their applications, especially for cleaning effect. For example, charge separation or accumulation may help clean the selected particles. Moreover, the droplets may change the electric potential of the treated object, which may affect surface conditions and dielectric properties [16]. The current flow of the mist was measured to understand the charge distribution and generation mechanism.

The mist is regarded as a stable flow, and its electrical characteristics are homogeneous, such that the electric current is stable during one record. Five samples were recorded in 2 s to determine the average. The average values were defined as the current under the measurement condition. The current as a function of distance with different inlet gas pressures and the current as a function of pressure at a distance of 2 mm are shown in Figs. 6 (a) and (b), respectively. The current value gradually reduces to zero with an increase in distance and increases with an increase in pressure.

6. Conclusion

In this study, a novel high-speed mist-generating device was developed based on the principle of the condensation of water vapor in pressurized air. The cleaning effect of the mist was validated by cleaning process indicators, and it was found that the material on the indicator was completely removed in less than 10 s at a distance of 1 cm from the nozzle when the gas pressure was greater than 4 atm. An inlet gas pressure of 5 atm and water temperature of 153 °C were recommended for this study. Thus, the distributions of the temperature and pressure were measured in the range of 35–49 mm along the x direction. Based on the experimental results, the mist velocity distribution was estimated to be 52–65 m s^{-1} at 35 mm and 40–51 m s^{-1} at 49 mm. The Schlieren method was used to visualize the mist flow at the nozzle exit. In this study, it was found that the gas and mist flows were underexpanded supersonic flows. The electric current on the metal plate near the supersonic region was measured. The current decreased with an increase in the distance from the nozzle exit and increased with an increase in the inlet gas pressure. This phenomenon might be caused by charge separation in the mist flow or owing to friction with or impact on the plate. Further analyses are required to clarify the generation mechanism of the current and influence of the droplet size and velocity.

Acknowledgment

This study was partly supported by the Priority Collaborative Research Project of the Institute of Fluid Science, Tohoku University (Project Code: J19J002, J20J001, J21J001). We would like to thank Prof. M. Watanabe (Hokkaido University), Prof. H. Yui (Tokyo University of Science), Prof. T. Yano (Osaka University), Assoc. Prof. K. Kobayashi (Hokkaido University), Prof. S. Fujimura (Tohoku Medical and Pharmaceutical University), Prof. Y. Iga (Tohoku University), Assoc. Prof. T. Sanada (Shizuoka University), and the Chief Research Officer K. Urashima (National Institute of Science and Technology Policy, MEXT) for the academic support.

References

[1] Slot D. E., Van Der Weijden G. A., and Dörfer C. E., The efficacy of interdental brushes on plaque and parameters of periodontal inflammation: a systematic review, *Blackwell Munksgaard Int J Dent Hyg*, Vol. 6, pp. 253− 264, 2008.
[2] Sheiham A., and Netuveli G. S., Periodontal diseases in Europe, *Periodontol 2000*, Vol. 29 (1), pp. 104−121, 2002.
[3] Choo A., Delac D. M., and Messer L. B., Oral hygiene measures and promotion: Review and considerations, *Aust Dent J*, Vol. 46 (3), pp. 166−73, 2001.
[4] Lang N. P., Cumming B. R., and Löe H., Toothbrushing frequency as it relates to plaque development and gingival health., *J Periodontol*, Vol. 44 (7), pp. 396−405, 1973.
[5] Hansen F. and Gjermo P., The plaque-removing effect of four toothbrushing methods, *Eur J Oral Sci.*, Vol. 79 (4), pp. 502−506, 1971.
[6] Frandsen A. M., Barbano J. P., Suomi J. D., Chang J. J., and Burke A. D., The effectiveness of the Charters', scrub and roll methods of toothbrushing by professionals in removing plaque, *Eur J Oral Sci.*, Vol. 78 (1−4), pp. 459−463, 1970.
[7] Nemcovsky C. E. and Artzi Z., Erosion-abrasion lesions revisited, *Compend Contin Educ Dent*, Vol. 17 (4), pp. 416−8, 420−3, 1996.
[8] Sälzer S., Slot D. E., Van Der Weijden F. A., and Dörfer C. E., Efficacy of inter-dental mechanical plaque control in managing gingivitis - A meta-review, *J Clin Periodontol*, Vol. 42 (S16), pp. S92−105, 2015.
[9] Sharma N. C., Lyle D. M., Qaqish J. G., and Schuller R., Comparison of two power interdental cleaning devices on the reduction of gingivitis, *J Clin Dent*, Vol. 23 (1), pp. 22−26, 2012.
[10] Rmaile A., Carugo D., Capretto L., Aspiras M., Jager M. D., Ward M., Stoodley P., Removal of interproximal dental biofilms by high-velocity water microdrops, *J Dent Res*, Vol. 93 (1), pp. 68−73, 2014.
[11] Stauff I., Derman S. H. M., Barbe A. G., Hoefer K. C., Bizhang M., Zimmer S., and Noack M.J., Efficacy and acceptance of a high-velocity microdroplet device for interdental cleaning in gingivitis patients—A monitored, randomized controlled trial, *Int J Dent Hyg.*, Vol. 16 (2), pp. e31−e37, 2018.

[12] Uehara S., Nakajima T., Moriya S., Maruyama S., and Sato T., Removal mechanism of artificial dental plaque by impact of micro-droplets, *ECS J Solid State Sci Technol.*, Vol. 8 (2), pp. N1−N5, 2019.
[13] Cense A. W., Van Dongen M. E. H., Gottenbos B., Nuijs A. M., and Shulepov S. Y., Removal of biofilms by impinging water droplets, *J. Appl. Phys.*, Vol. 100 (12), 124701, 2006.
[14] Linden P. F., and Simpson J. E., Gravity-driven flows in a turbulent fluid. *J. Fluid Mechanics*, Vol. 172, pp. 481−497, 1986.
[15] Husted B. P., Petersson P., Lund I., and Holmstedt G., Comparison of PIV and PDA droplet velocity measurement techniques on two high-pressure water mist nozzles, *Fire Safety J.*, Vol. 44 (8), pp. 1030−1045, 2009.
[16] Baret J. C., and Mugele, F., Electrical discharge in capillary breakup: controlling the charge of a droplet, *Phys. Rev Lett*, Vol. 96 (1), 016106, 2006.
[17] Ryushi T., Kita I., Sakurai T., Yasumatsu M., Isokawa M., Aihara Y., and Hama K., The effect of exposure to negative air ions on the recovery of physiological responses after moderate endurance exercise. *Int. J. Biometeorol.*, Vol. 41 (3), pp. 132−136, 1998.
[18] Wei Z., Li Y., Cooks R. G., and Yan X., Accelerated reaction kinetics in microdroplets: overview and recent developments, *Annu Rev Phys Chem.*, Vol. 71, pp. 31−51, 2020.
[19] Lee J. K., Walker K. L., Han H. S., Kang J., Prinz F. B., Waymouth R. M., Nam H.G., and Zare R.N., Spontaneous generation of hydrogen peroxide from aqueous microdroplets, *Proc. Natl. Acad. Sci. USA*, Vol. 116 (39), pp. 19294−19298, 2019.
[20] Lee J. K., Han H. S., Chaikasetsin S., Marron D. P., Waymouth R. M., Prinz F. B.,and Zare R.N., Condensing water vapor to droplets generates hydrogen peroxide, *Proc. Natl. Acad. Sci. USA*, Vol. 117 (49), pp. 30934−30941, 2020.